STATE OF OREGON
DEPARTMENT OF GEOLOGY AND MINERAL INDUSTRIES
910 State Office Building
Portland, Oregon 97201

OPEN-FILE REPORT O-86-15

OCEAN BOTTOM SEISMOMETER MEASUREMENTS ON THE GORDA RIDGE

By L. Dale Bibee,
College of Oceanography, Oregon State University,
Corvallis, Oregon 97331

Final Report for Contract No. 63-630-8510

Submitted to:
Oregon Department of Geology and Mineral Industries
and the
Gorda Ridge Technical Task Force

Released July 1986

NOTICE

This report is based on results of a research program directed by the joint federal-state Gorda Ridge Technical Task Force, managed by the Oregon Department of Geology and Mineral Industries, and funded by the Minerals Management Service, U.S. Department of the Interior, through Cooperative Agreement. Opinions expressed are those of the authors and do not constitute endorsement by the sponsoring agencies or the Task Force.

The Oregon Department of Geology and Mineral Industries is publishing this paper because the subject matter is consistent with the mission of the Department. To facilitate timely distribution of information, camera-ready copy submitted by the authors has not been edited by the staff of the Oregon Department of Geology and Mineral Industries.

Contents

List of figures

Abstract

Ocean bottom seismometer measurements on the southern Juan de Fuca Ridge and the southern Gorda Ridge show both areas to be seismically active. Swarms of earthquakes coupled with low frequency tremor characterize the seismicity of the the Southern Juan de Fuca, and are probably associated with the volcanic system on the ridge axis. The frequency of occurrence of earthquakes on the southern Gorda Ridge is lower than that on the northern Gorda Ridge or the Juan de Fuca Ridge, but numerous earthquakes were recorded. The epicenters of earthquakes correlate with faults and volcanic centers observed on seismic reflection records. These active faults are likely zones of hydrothermal circulation and sulfide deposition because they provide permeable pathways for fluid flow. Seismic refraction measurements on the southern Juan de Fuca Ridge suggest that the basalt within 1.2 km of the seafloor is highly porous, thus allowing efficient flow of hydrothermal fluids.

Introduction

In July, August, and September of 1985 seismic experiments were carried out on the southern Juan de Fuca Ridge and the southern Gorda Ridge. The goal of these experiments was to characterize the seismicity and seismic structure associated with a midocean ridge hydrothermal vent field and to use those characteristics to help locate potential sites of venting. There is increasing evidence that many ridgecrest vent systems are associated with active fault systems that provide a permeable pathway for fluid circulation (Rona et al., 1986). In addition, magmatic systems that provide the heat source for hydrothermal systems are known to generate significant seismic activity. The delineation of active areas using a microseismic network of ocean bottom seismometers was the primary objective of the work described here.

Instrumentation

The major tool for microseismic surveys in the ocean is the ocean bottom seismometer (OBS). During the experiments described here 3 different types of OBS were used . The first type records data from a vertical and one horizontal geophone, a hydrophone, and time code on magnetic tape in a continuous analog fashion. It has the advantage that a continuous record is produced, but suffers from limited dynamic range, frequency response and recording fidelity. Stations labeled S3, S14, and S23 use instruments of this type. A second type of instrument contains a microprocessor system that digitally records data from a vertical geophone, 2 orthogonal horizontal geophones, and a hydrophone. It has the advantage of recording all three components of ground motion with superior fidelity, but has limited recording time. Data is thus selectively recorded based on either predetermined recording windows or on a trigger system which compares the current signal with the average background noise and triggers recording when large signals are detected. Selecting an algorithm which records the desired events but excludes noise bursts is the most difficult part of setting up this system. Stations labeled S21 and S22 are of this type. The third type of instrument is really a variation of the second type. The digital recording system is identical, but the only sensor is a hydrophone. The package of geophone sensors for this instrument was lost on a cruise leg just prior to this work and could not be replaced in time. Stations labeled S20 are of this type.

All of the instruments are deployed in a similar package. The instrument pressure case and floatation spheres are attached to a framework which is in turn attached to a cement anchor with dual burn wire releases. The package is allowed to free-fall to the seafloor. At recovery time the anchor is released and the package returns to the surface. Release can be triggered either by acoustic command or by dual internal timers. All units have acoustic transpond capability, and the digital units can also transmit diagnostic information acoustically from the seafloor.

Field Operations

Ocean bottom seismometers were deployed on two cruise legs of the S. P. LEE during the summer of 1985. The ship left Redwood City, Ca. July 27 and proceeded directly to the southern Juan de Fuca Ridge. The work area was centered at 44° 40' N latitude and 130° 20' W longitude. Previous investigations had shown the existence of at least 5 active vents in this area. Ocean bottom seismometers were deployed in the pattern shown in figure 1. Three were placed along the axis of the ridge (S20, S21, and S23). S20 and S21 were placed on the sheet flows of the rift valley adjacent to the axial cleft inside of which the known vents are located. S23 was dropped into the cleft itself. S3 and S14 were deployed approximately 5 km off-axis in the bordering hills. Deployment operations were hindered by heavy weather which made laboratory

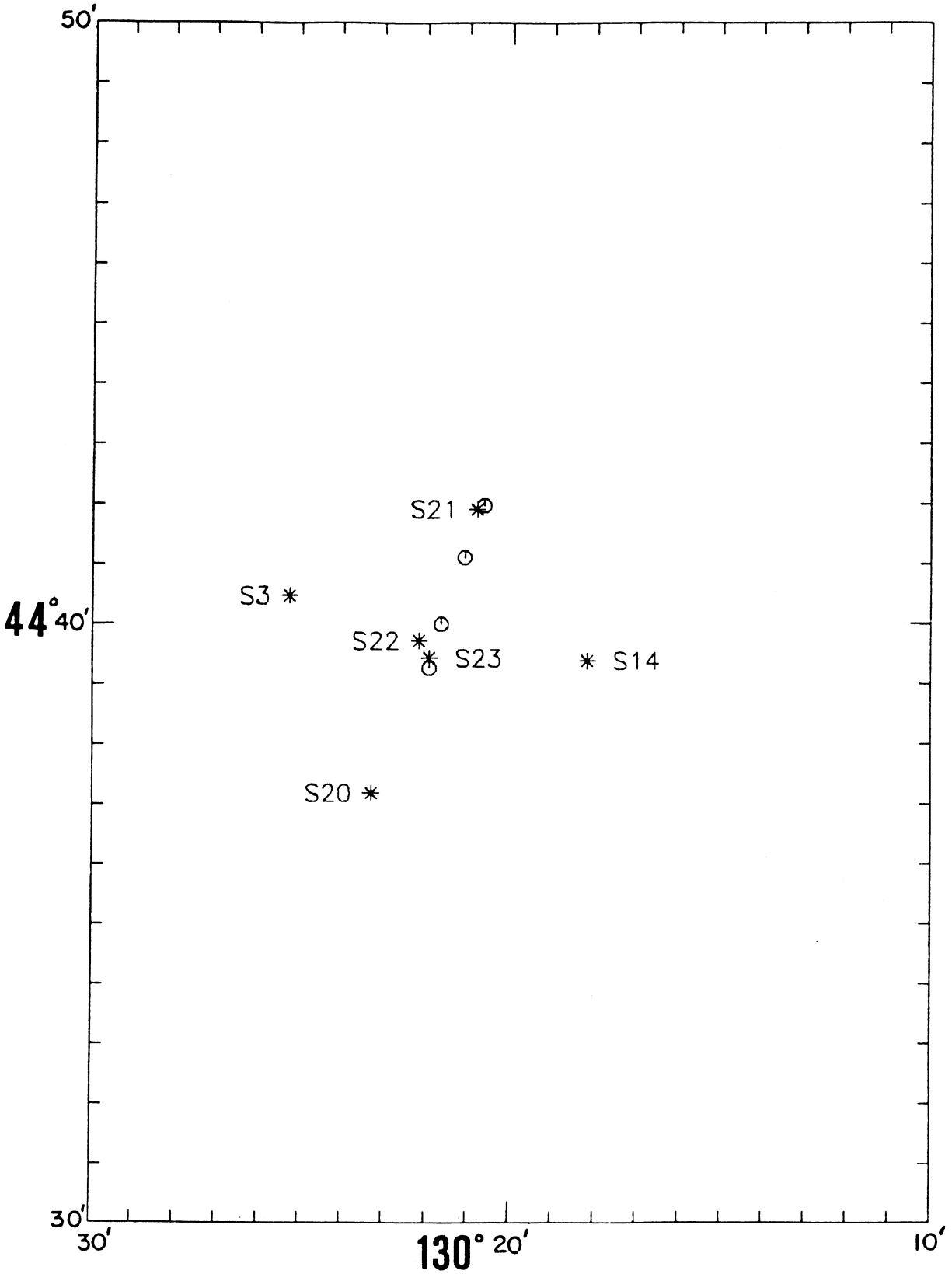

Figure 1. Locations of ocean bottom seismometers deployed on the southern Juan de Fuca Ridge. The circles are identified sites of hydrothermal venting. S21, S22, and S20 were digital recording instruments. S14 and S23 were analog continuous recording instruments. S3 was not recovered.

operations, deck work, and ship positioning difficult.

After deployment of the first 5 units, 2 refraction profiles were shot using an array of airguns with approximately 1500 cubic inches of total capacity. One profile was shot along the axis of the ridge and the second was shot perpendicular to the ridge. After the refraction shooting, a sixth ocean bottom seismometer was deployed (S22) near the center of the area. Again this unit was placed on the sheet flows adjacent to the axial cleft. After additional unrelated operations were conducted in the Blanco Fracture Zone, the S. P. LEE returned to the area to recover the ocean bottom seismometers. All units except S3 were recovered. S3 did not surface at the appropriate time and there was no acoustic contact. Given the reliability of the release mechanism (this was the only loss in 21 deployments this summer) and the redundancy of systems, the most probable cause for the loss was that the unit had surfaced earlier and floated away. Possibly this happened right after deployment when impact with the bottom might have broken the anchor loose. While we were in the general area after launch, the heavy sea conditions probably would have prevented us from spotting the instrument at the surface.

Data recovery on the recovered instruments was in general poor. S14 functioned correctly and provides a continuous data record throughout the deployment. S21 recorded the refraction profiles, and a small number of seismic events triggered recording. However it stopped triggering shortly after the refraction work. S22 recorded a series of events immediately after deployment, but then its tape drive jammed. Times of triggering events were still recorded in its computer memory and recovered so that we have a record of activity frequency, but we have waveforms recorded on only the first few events. S20 collected no data because an insulating connector was left off at deployment time. The computer reset as the instrument hit the water. S23 developed a tape recorder problem just after deployment and recorded no data. In summary, one instrument recorded a complete record and 2 other instruments recorded partial records. Despite these problems, the data recovered provide a valuable and interesting data set.

The second cruise leg left Newport, Oregon on September 3. We proceeded directly to the work area on the southern Gorda Ridge at 41° N latitude and 127° 30' W longitude. We immediately began deployment of 5 ocean bottom seismometers, interspersed with coring and seismic reflection operations. Figure 2 shows the distribution of seismometers for this deployment. The instruments were spaced approximately 15 km apart in an attempt to do a reconnaissance level survey. Unlike the northern Gorda Ridge for which this project was originally proposed, we had no previous data to allow us to concentrate our efforts on one area. By expanding the array, we were trading off location accuracy and earthquake magnitude detection threshold for areal coverage. After being in place for 6 days, the instruments were recovered.

S21A and S14A both recorded throughout the period. S23A recorded for about 18 hours after deployment before it suffered a tape jam. Unfortunately, it was the first instrument deployed and thus provided recording overlap of only about 10 hours with S14A and no overlap with S21A. S22A and S20A both suffered tape jams and recorded no waveforms, however both recorded the times of triggering events and therefore provided data on activity frequency levels. The problem of tapes jamming was particularly perplexing. Before this summer's work it had happened only twice in all of our work dating back to 1980. We were never able to duplicate this failure mode in the laboratory. Before redeploying the instruments, we conducted some tests in the refrigerated core van. These showed that the source of the problem was a plastic insert in a pulley that loosened under low temperature conditions due to differential

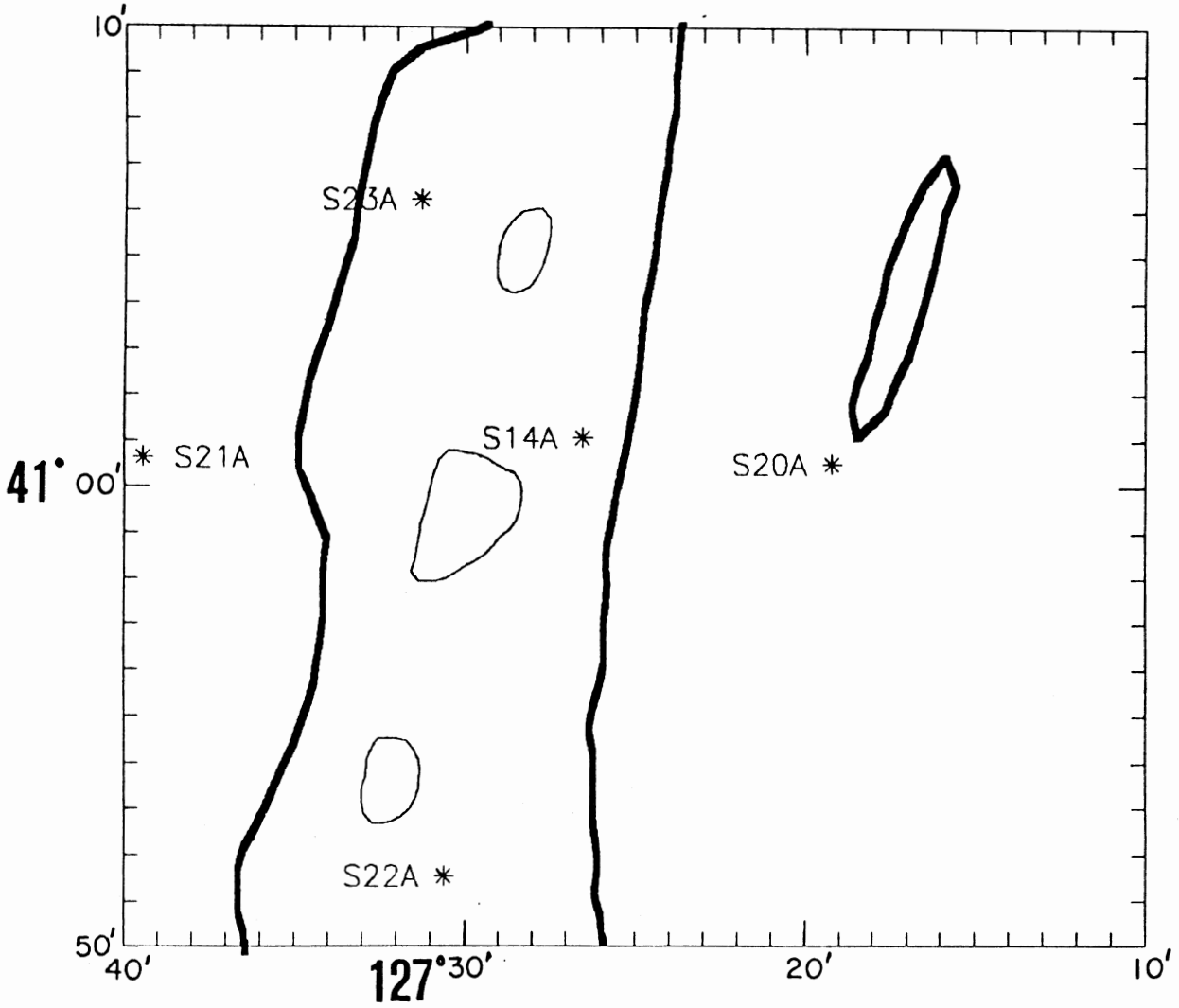

Figure 2. Location of ocean bottom seismometers deployed on the southern Gorda Ridge on the initial deployment. The dark lines are the 3000 meter contours that define the axial valley. The light outlines are volcanic edifices identified from seismic reflection records.

shrinkage. A small amount of epoxy fixed the problem.

Since the data from the first deployment did not conclusively show any "hotspots" of seismic activity on initial inspection, we decided to redeploy a second smaller network in the same area, where we could take advantage of the transponder network deployed for camera and heat flow work. Figure 3 shows the location of instruments in the second network. After deployment, a set of two refraction profiles were shot using the airgun array source. One profile was oriented along the ridge axis and the other was oriented perpendicular to it. After about 4 days the instruments were recovered. S21B, S20B, S23B, and S14B recorded perfectly throughout the deployment. S22B recorded the refraction data on all but the vertical geophone channel. Since unscheduled events are triggered on the vertical channel, which was not working, no triggering events were recorded on this instrument.

Data Reduction and Analysis

Unlike many methods of geophysical surveying that provide real-time records for interpretation, the data tapes from ocean bottom seismometers require substantial processing before the information can be evaluated. This processing can only be accomplished by putting the data in a computer compatible form. For the data from digital instruments this is less of a problem. The data is already recorded on the field tapes in digital form and needs only to be transcribed to standard computer media (9-track tape).

However the analog recorded data needs to be digitized by a computer system. Since it is impossible to digitize the continuous record (this would require hundreds of tapes), we must first select the data to convert. We do this in the same way that an instrument operating on the seafloor would; that is by using an event detection algorithm. A master list is then created from triggering events occurring on any of the instruments (digital and analog) and the portions of the analog tapes corresponding to the list are digitized. After corrections for instrument clock drift, the transcribed digital tapes and the digitized analog tapes are used as the data base for all future analysis.

Analyses of the refraction and seismicity data are very different after this point. For refraction data, the known origin time and location of the source is combined with the recorded data to form a record section showing the change in travel time and waveform with shot-receiver separation. Travel times of the phases are then picked from an interactive graphics terminal and, after correction for bathymetry and sediment thickness, are inverted for seismic velocity as a function of depth.

For the seismicity data, seismograms are plotted on a graphics terminal and, where the data are of sufficient quality, phases are identified and their arrival times at the stations picked. These arrival times are then used to locate the earthquake using a computerized location program. The data are often insufficient to determine an actual location, but contain information about the distance of the event from a given station or the azimuth from the epicenter to the network. Additional information concerning the subsurface velocity structure is necessary for computation of the location. This information is provided by the seismic refraction lines and, in the case of the sedimented southern Gorda Ridge, from the seismic reflection profiles.

Results

Southern Juan de Fuca Ridge

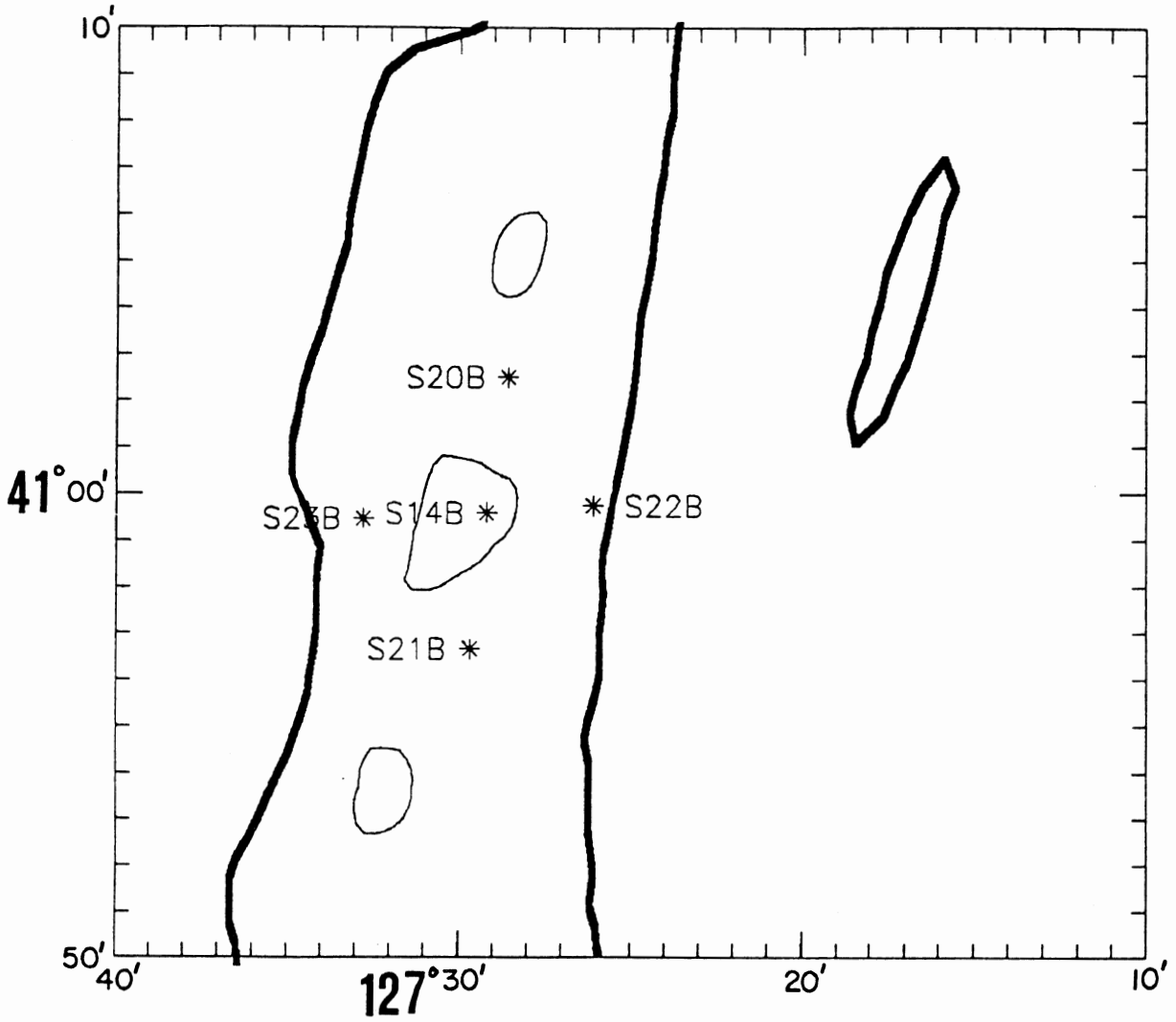

Figure 3. Location of ocean bottom seismometers deployed on the southern Gorda Ridge on the second deployment. The dark lines are the 3000 meter contours that define the axial valley. The light outlines are volcanic edifices identified from seismic reflection records.

Figure 4 shows a plot of the observed seismic activity levels on the southern Juan de Fuca Ridge. The instrument at station S14 provides the best record of activity levels because it recorded continuously. Typical background levels are about one triggering event per hour. During a 24 hour period on August 2 and 3 recorded levels reached almost 200 events per 6 hour period. Figure 5 is a section of the waveform recorded from a vertical geophone at the beginning of this activity, and shows that the activity is almost continuous. In fact, the levels shown in figure 4 are an underestimate of the actual number of events because the event detection algorithm considers all triggers detected within a 30-second window as a single event. Identifying phases that would allow one to constrain the location of these events is very difficult because of interference from multiple events. However, the waveforms are not inconsistent with the events having occurred on the ridgecrest at a distance of 5 km from S14.

S22 was deployed in during the middle of this swarm of activity. The pattern of event triggers on that instrument also indicates a peak in activity early on August 3. Comparison of the actual numbers of triggers on S22 and S14 is not valid as an indication of the relative activity levels in the two areas because the event detection algorithms for the digital and analog systems are different. However the data from S22 do provide evidence for an earthquake swarm in the area on August 3.

The waveforms from the events recorded on S22 before the tape jammed are extremely interesting (Figure 6). In addition to high frequency (>5 hz) signals normally associated with microearthquakes, there is a significant amount of low frequency (1-2 hz) energy. In some cases this energy appears to be a general background noise upon which the high frequency signals are superimposed, but in other cases, it appears to start at the same time as the high frequency signals. Such low frequency signals have been observed on subaerial volcanic systems in the form of harmonic tremor and low frequency earthquakes. At Mt. St. Helens these types of signals have been observed only in conjunction with eruptive cycles (Fehler and Chouet, 1982). The low frequency energy is generally thought to be caused by a resonance phenomenon in magma filled cracks or chambers (Chouet, 1981). Therefore one explanation for our the August 3 event is that it represents the intrusion or eruption of magma along the ridgecrest. The low frequency in the earthquake may be caused by resonance in a fluid filled crack and the high frequency bursts may be caused by fracturing associated with the propagation of that crack.

The instrument at S21 recorded only 8 event triggers because during most of its recording period it was operating in window mode for the refraction shooting. However, those events that it did record look very much like those at S22 in that they display significant amounts of low frequency energy. We have not observed events of this type at any other location. Since both S21 and S22 are very close to active hydrothermal vents, we cannot exclude the possibility that the anomalous earthquakes are associated with the hydrothermal systems rather than directly with the magmatic system. However, the recording of swarm activity by the off-ridge instrument (S14) indicates that the source of the activity need not be immediately adjacent to the recording station.

The refraction data from S21 are of particularly high quality. Very few refraction surveys have been successfully completed directly on a ridge axis because of generally rough bathymetry. The data set that we obtained along the flat lava plain is one of the best yet collected for studying uppermost crustal structure at the ridge axis. Figures 7, 8, 9, and 10 show record sections of the raw data for the line shot along the ridge axis. The presence of low frequency noise (possibly tremor) can be seen in the profile shot to the south of the instrument. To both the north and

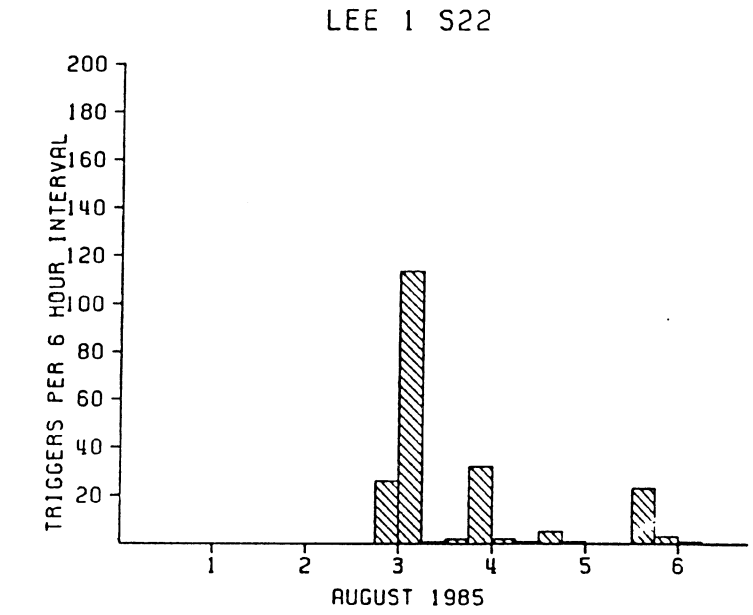

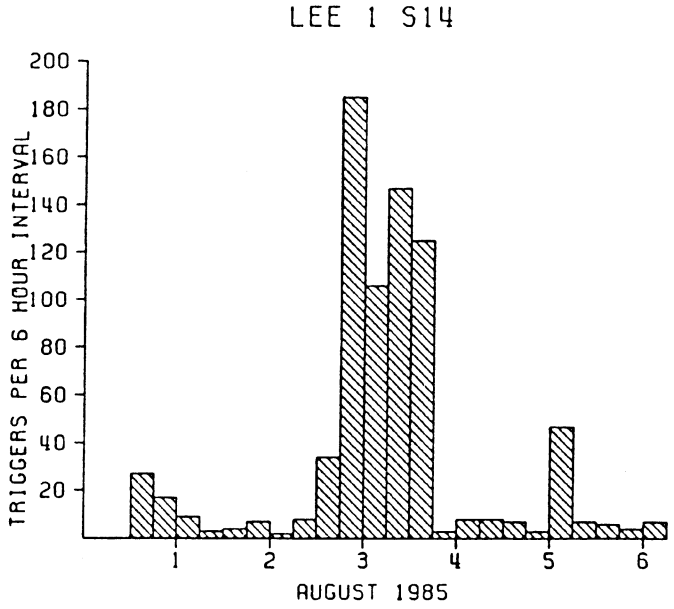

Figure 4. Histograms of activity levels recorded on the southern Juan de Fuca Ridge. The large peak on August 3 is an intense earthquake "swarm".

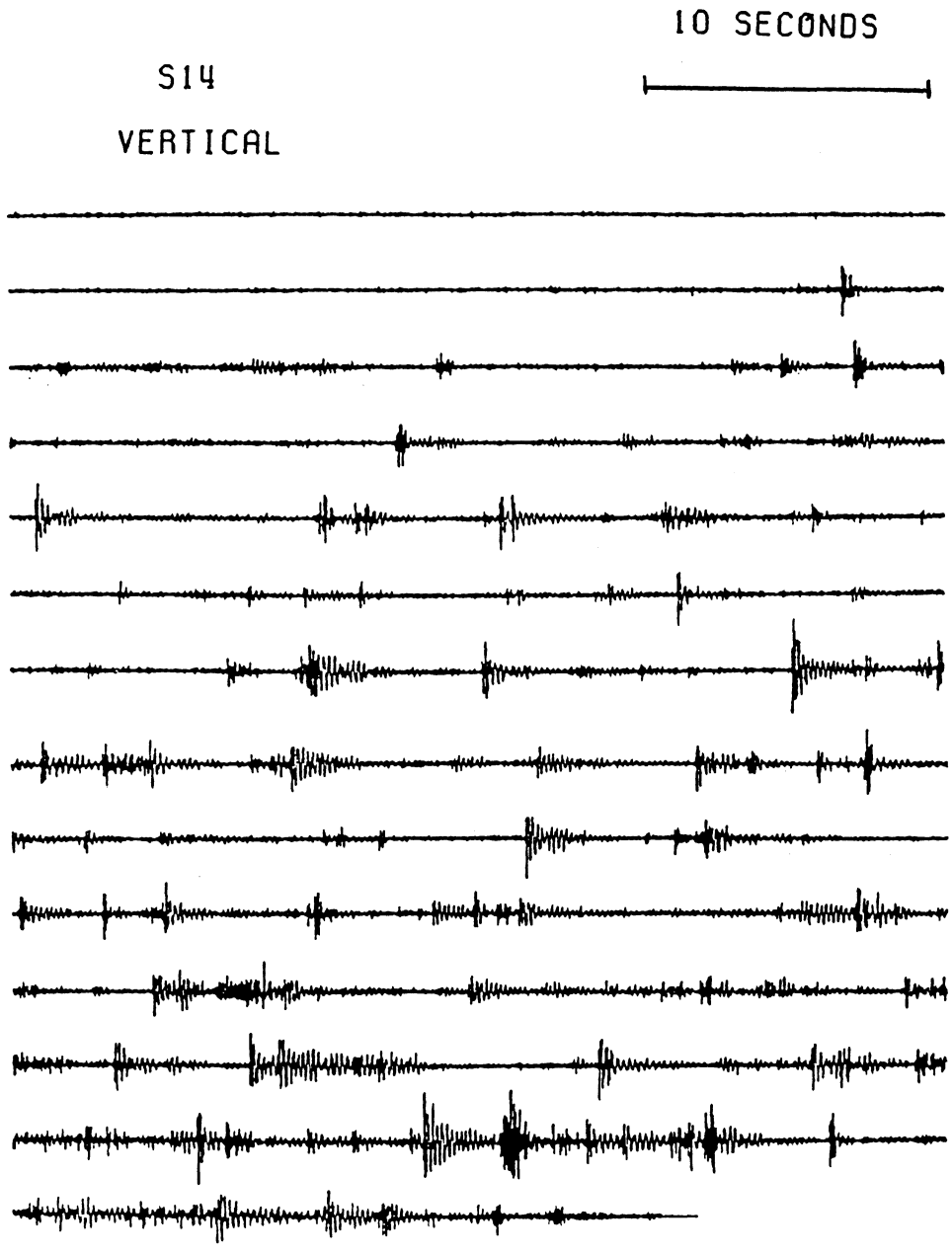

Figure 5. Waveforms recorded on the vertical geophone of S14 at the beginning of the swarm noted in figure 4. Each line represents 30 seconds of data with time increasing from left to right and top to bottom. Almost 7 minutes of data are displayed. Note the almost continuous activity.

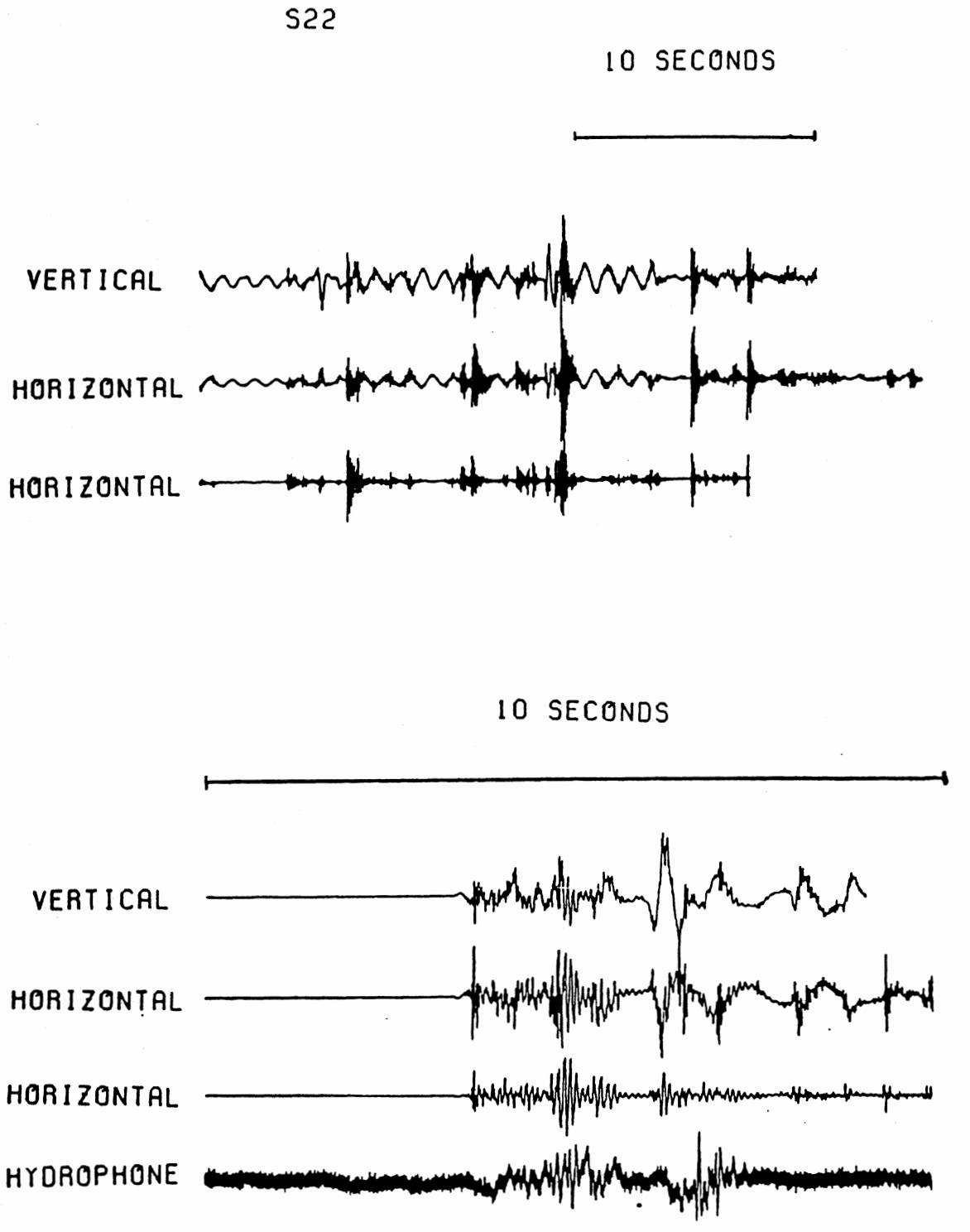

Figure 6. Waveforms recorded on S22 (ridge axis) during the earthquake swarm activity. Two separate events are shown. In the upper event, high frequency bursts are superimposed on a low frequency tremor-like signal. In the lower event, the low frequency signal seems to start at the same time as high frequency signal. This behavior is similar to that of long period earthquakes from subaerial volcanic systems.

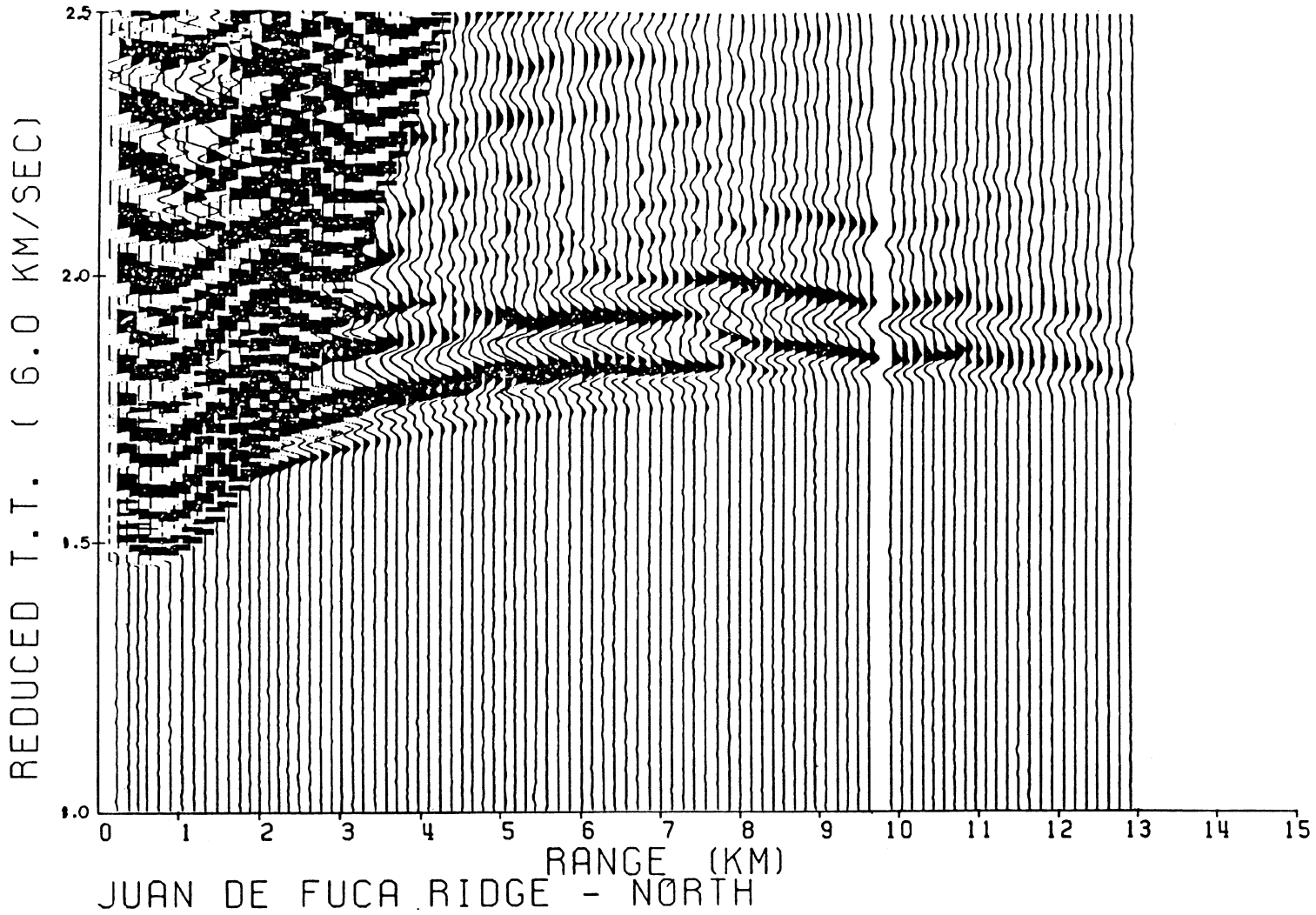

Figure 7. Reduced time record section of refraction data from S21. The shots on this line are to the north of the instrument. The energy at about 1.8 seconds between 2 and 13 km is being refracted as a compressional wave through the upper 2 km of the crust. This is a vertical geophone recording.

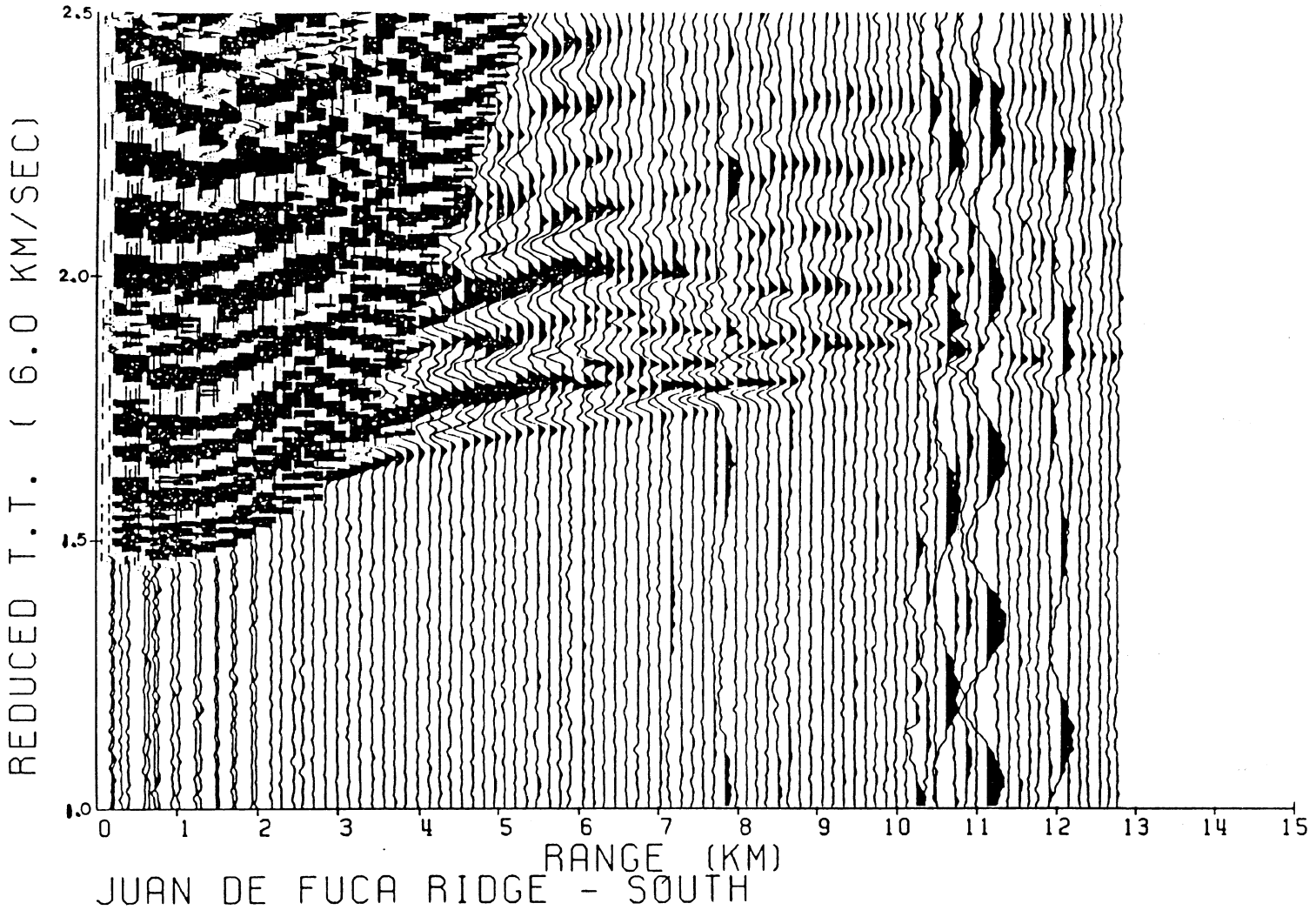

Figure 8. Reduced time record section of refraction data from S21. The shots on this line are to the south of the instrument. The energy at about 1.8 seconds between 2 and 13 km is being refracted as a compressional wave through the upper 2 km of the crust. This is a vertical geophone recording.

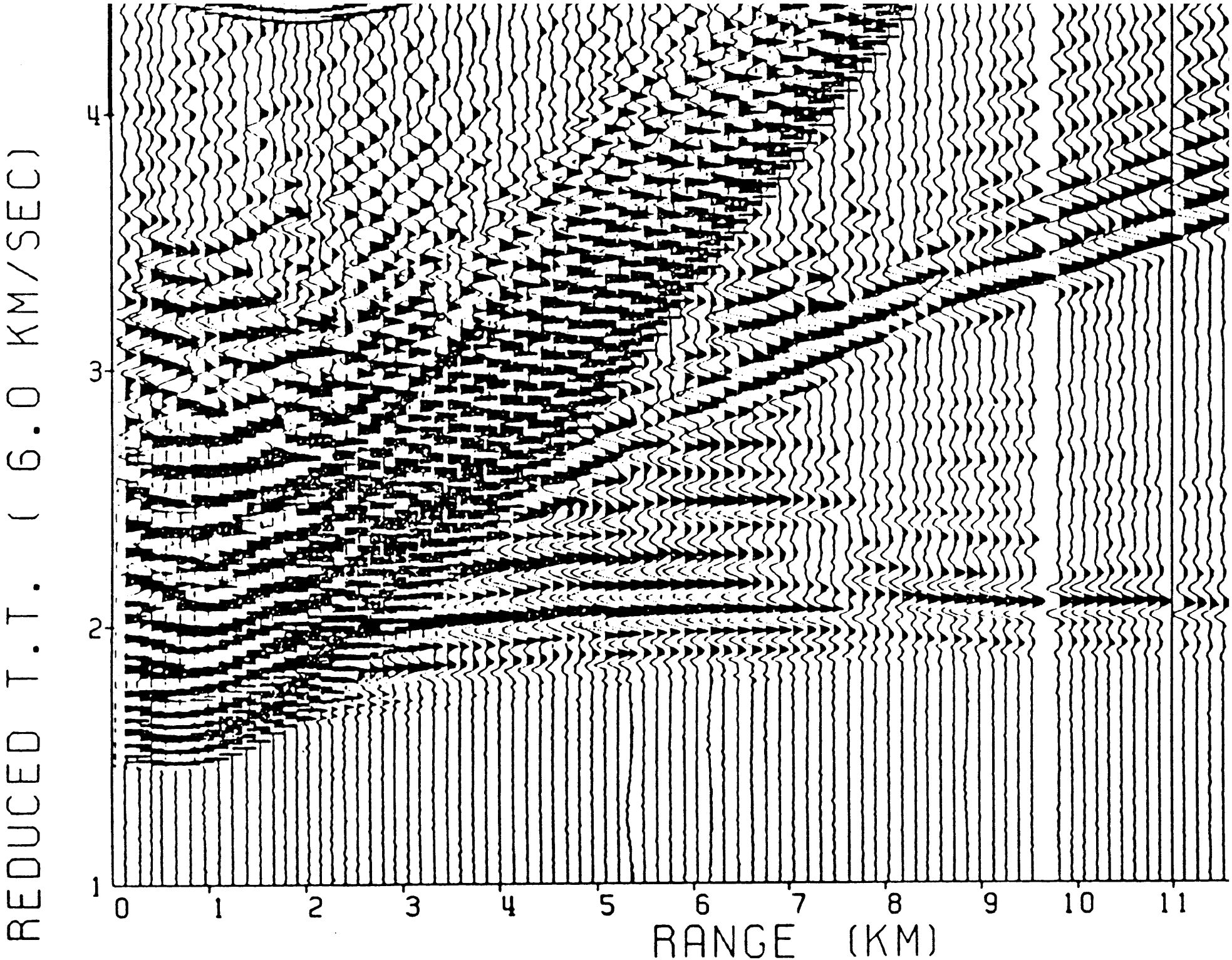
REDUCED T. T. (6.0 KM/SEC)
4
3
2
1
0
1
2
3
4
5
6
7
8
9
10
11
RANGE (KM)

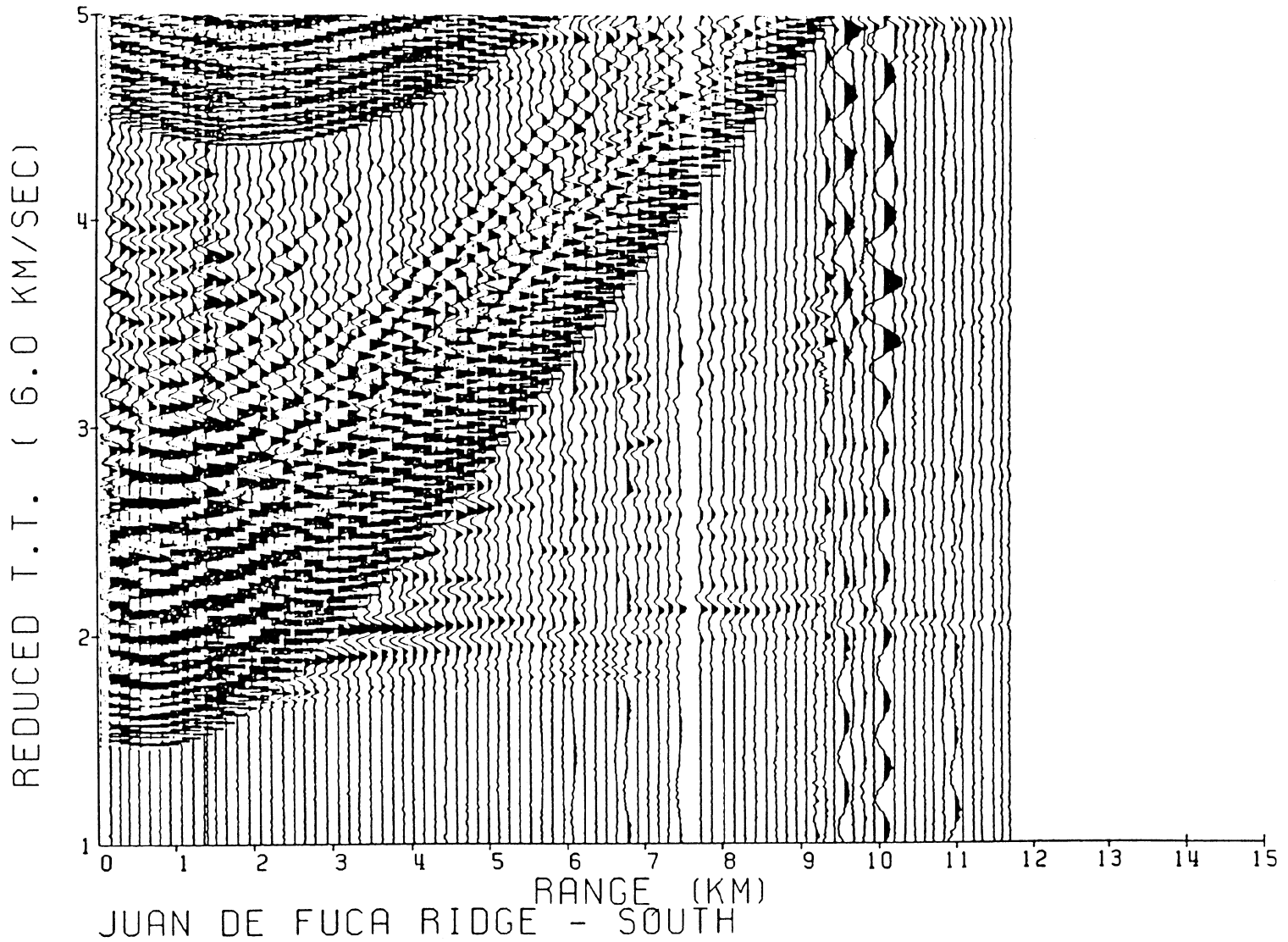

Figure 10. Reduced time record section of refraction data from S21. The shots on this line are to the south of the instrument. The energy between 4 and 13 km at about 3 seconds is traveling as a shear wave through the upper crust. This is a horizontal component recording.

south of S21 we see a similar pattern. The direct water arrival is the first arriving phase for the first 1.5 km of the profile. From 1.5 to 8 km the first arrival is a wave refracted in the basalt. A curve connecting the first observable signal on each seismogram has a concave downward shape, which requires a gradual increase in seismic velocity with depth. At about 8 km range the first arrival decreases in amplitude below the noise level and a later phase with higher phase velocity becomes the first arrival. This requires a sharp decrease in the velocity gradient at the depth to which the rays are penetrating. The velocities may even decrease beyond this depth. Still deeper the velocity must again increase to generate the energy beyond 8 km.

Decreases in velocity with depth have been suggested as indicators of magma reservoirs at depth below ridgecrests (e.g. Orcutt et al.,1976). However, figures 9 and 10 suggest that this is not the cause of the velocity structure responsible for the amplitude decrease at 8 km. The figures show the observed horizontal component of ground motion and clearly show shear waves that propagate through this part of the crust. A magma reservoir is unlikely to propagate shear waves and would need to be deeper than our profiles sample. Multichannel profiles across the ridge in this area show reflections from deeper levels in the crust that are interpreted as reflections from a magma reservoir (Morton and Sleep, 1985).

Although the data to the north and south of the OBS are similar in appearance, there are small differences. Figure 11 compares the first arrival travel times from both the north and south profiles. Arrivals from the north arrive slightly earlier at distances beyond 4 km range and show higher phase velocities over the same range. When these data are inverted for velocity structure (figure 12), the velocity differences become apparent at depths below 500 meters.

Because of the experimental geometry (surface sources), no rays are observed as first arrivals that turn in the upper 250 meters and return to the receiver without having sampled the lower seismic structure. We have modeled that region as a layer of constant velocity gradient. The travel time constraints of the deeper turning rays require the velocity at the seafloor to be 2.5 km/s and to increase very rapidly to about 4.5 km/s at 250 meters depth. The velocity then increases more slowly down to a depth of about 1.2 km, where it stops increasing. The travel time data requires only that the velocity stop increasing, but the rapid decrease in amplitude of the signals at a shot-receiver separation of 8 km suggests that the velocity may even decrease below 1.2 km. At a depth of 1.5 km to the south and 2.0 km to the north, the velocity increases rapidly to 6.1 km/s in the south and 6.5 km/s in the north.

Velocities of massive (low porosity) basalts are typically 5.5 km/s. Aside from rock type and mineralogy, porosity and temperature are the two factors most responsible for controlling the velocity structure on the ridge. Higher porosities will tend to decrease velocity as will higher temperature. Beneath the ridge, temperature increases with depth and porosity is likely to decrease with depth, producing competing effects on velocity. These two factors are not independent. In areas of high porosity, temperature gradients are probably low because the circulation of water efficiently distributes the heat. The velocities in the upper 1.2 km of the crust must be controlled by porosity changes because our data shows a rapid increase in velocity with depth. At that depth, the seismic velocities are typical of very low porosity basalt which probably restricts the flow of hydrothermal fluids. The increase in velocity at depths of 1.5 to 2 km probably represents the transition from extrusives to a sheeted dike complex. The very low velocity at the seafloor indicates that the near surface basalts are highly porous. The lower velocities to the south (beneath the vent field) are consistent with higher thermal gradients and possibly a shallower heat source.

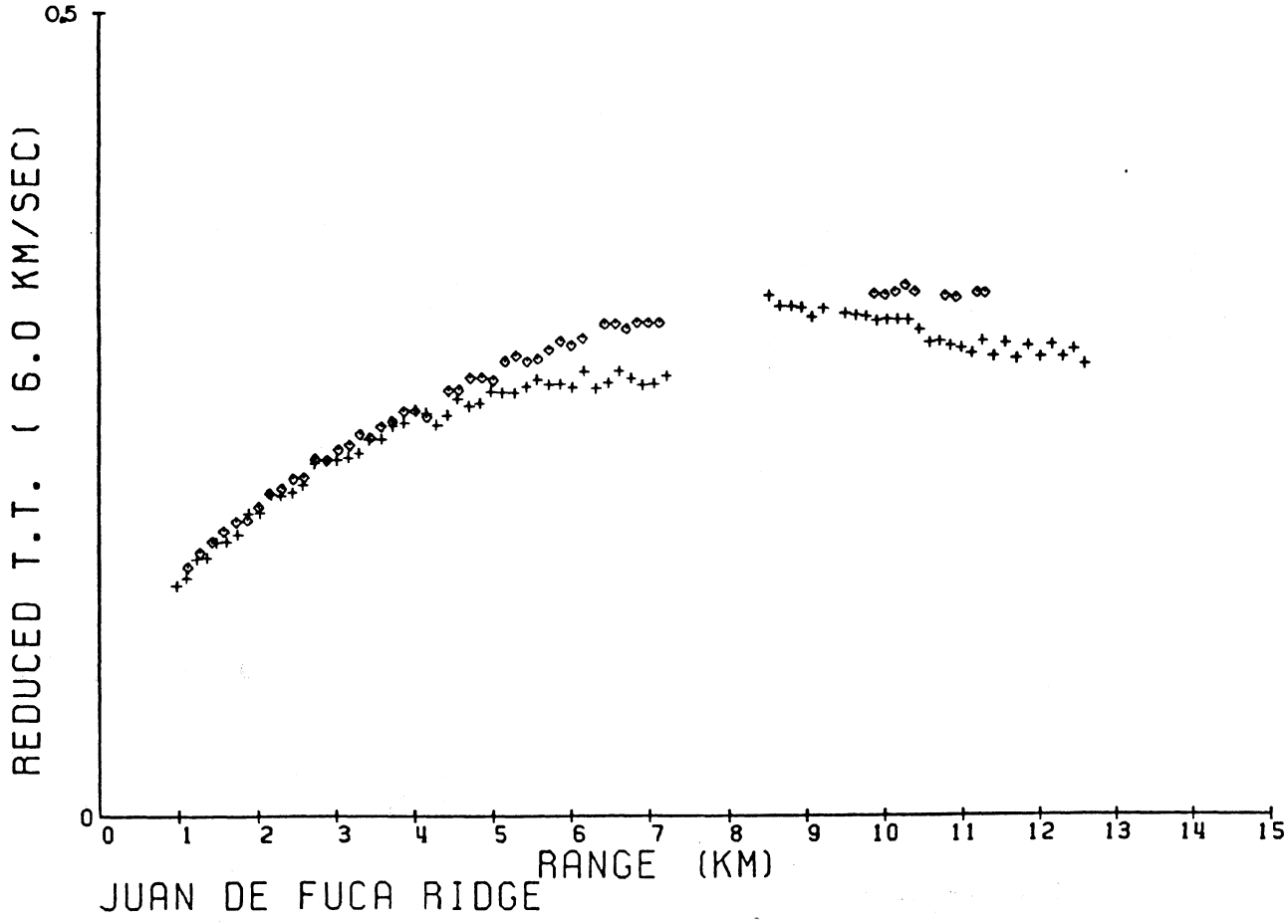

Figure 11. Travel time vrs. distance plot of first arrivals picked from figures 7 and 8. The diamonds are data from south of the instrument and arrive slightly later than the plus signs which represent data from the north. All travel times have been corrected for variations in bathymetry.

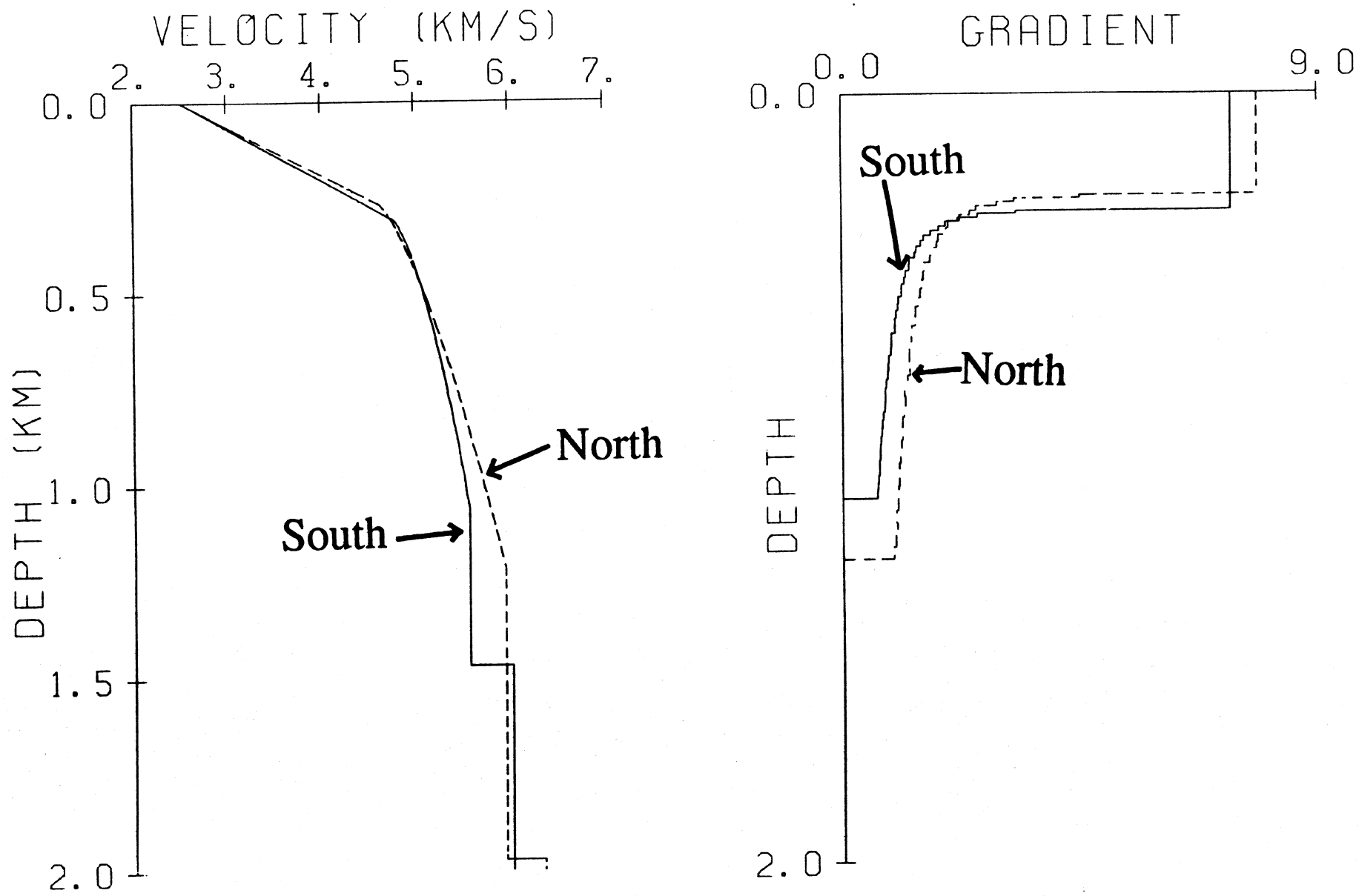

Figure 12. The velocity models derived from inverting the travel time data in figure 11. The profile to the north has higher velocities and velocity gradients than the structure to the south at depths between 0.5 and 1.5 km.

A further check on the velocity models is to evaluate amplitude levels. The higher velocity gradients to the north will turn more rays and should generate higher amplitude signals. Figure 13 compares the observed energy from the two profiles, and shows that the data from shots to the north of the OBS are considerably more energetic as expected.

These velocity models should provide useful input for additional processing of multichannel reflection data in the area.

Southern Gorda Ridge

Because of the complex sedimentary structure overlying the volcanic basement and the lower signal/noise ratio of the seismic refraction data in the Escanaba trough, a detailed velocity analysis similar to the one in the southern Juan de Fuca ridge is beyond the scope of this project. Instead, we have used the refraction data to verify the sediment thickness below the receivers determined from reflection data, and to calculate an average crustal velocity (6.5 km/s) for use in the earthquake location computations.

The location of earthquakes in this area was particularly difficult because of the variable sediment thickness. Conversions of P to S waves and S to P waves at the sediment-basement interface are particularly important to identify because the sediments contribute a large amount to the travel time (particularly for shear waves). With the triaxial geophone package of our digital instruments it was possible to identify these individual phases in most cases.

Figure 14 and 15 show the activity levels for all of the instrument deployments in the Escanaba trough. From the first deployed network, it is clear that highest seismic activity levels were measured in the trough as opposed to the adjacent hills. We digitized and reviewed 685 possible event triggers on the first deployment and 1008 for the second drop. Of these triggers only a very few were from local earthquakes. Many were emergent signals from tens of kilometers to the north, and many others were apparently due to local biological activity disturbing the instruments. We conclude that these disturbances were biological because there were large signals on the vertical and horizontal ground motion components but no signal at all on the hydrophone. Earthquakes invariably caused signals on all three components.

At the beginning of the first deployment only the instrument at S23A was in position. Of the recorded events, 6 were clearly earthquakes with nearly identical waveforms, indicating a common source point and mechanism. One of these events occurred after S14A was also deployed. It produced no signal on S14A, suggesting an origin to the north. The relative arrival times of P and S waves at S23A indicate that the source is located approximately 20 km away from S23A. If the source is on the ridge axis, then the earthquakes should be at a latitude of 41° 17' N. Given the limited data on these events, we can only speculate on the accuracy of this location. Two small event occurred very close (within 4 km) to S23A, but they were not recorded on any other instrument. Only in one case were we able to locate an event from the first deployment in a more quantitative way, using two events that had identical waveforms at S14A, indicating that they had the same origin. The first happened while S23A was operating but before S21A was in place. The second occurred when S21A was recording but after S23A stopped recording. Data from the two events recorded by the three stations located the events on the east wall of the axial valley at 40° 45' latitude. This approximate location is consistent with the times that the second event triggered S22A and S20A (although we don't have waveform records from those

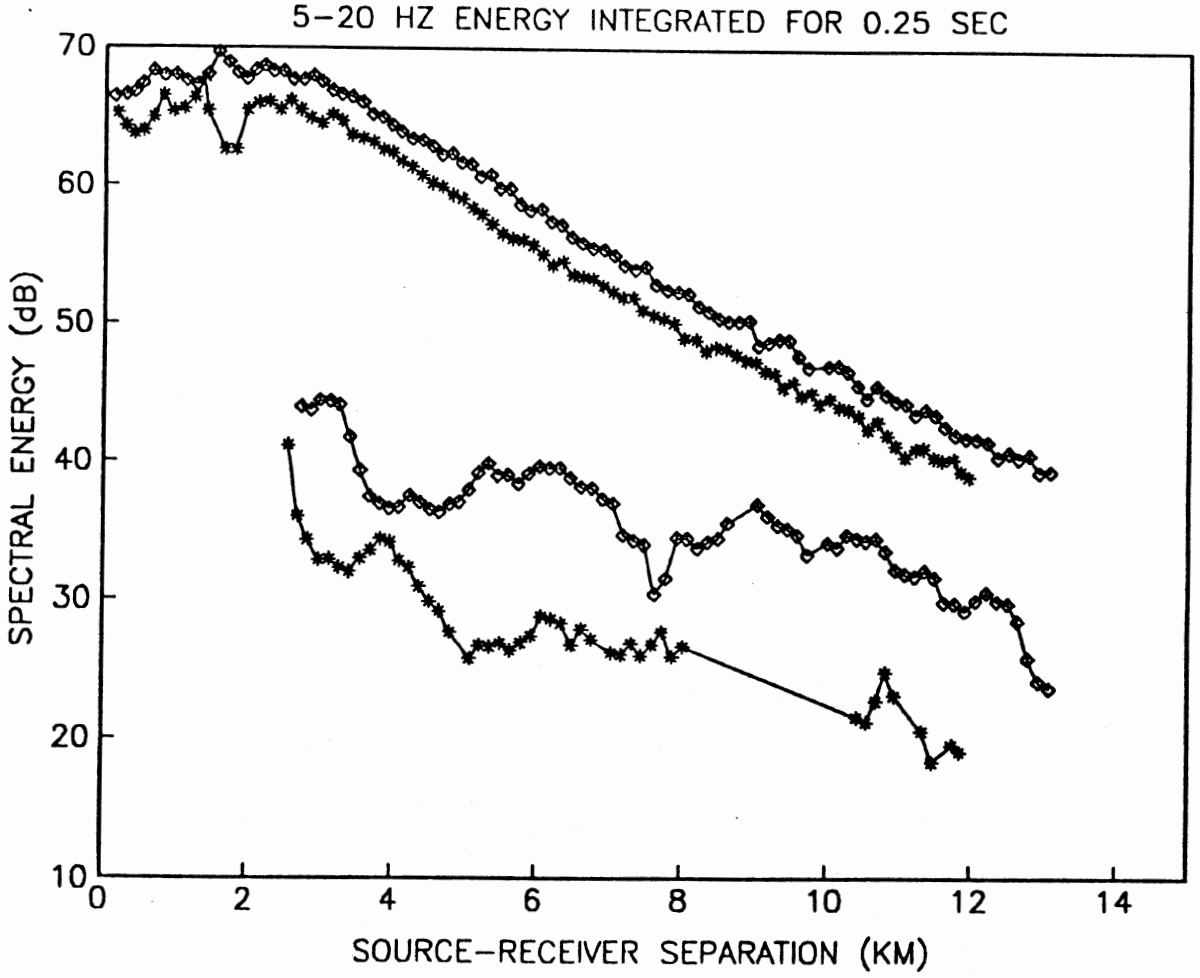

Figure 13. The energy in the compressional wave as a function of range. Diamonds are for data north of the receiver, stars are data south of the receiver. The upper two curves are the water borne energy and show only a small difference in energy. The lower curves are from the ground waves. They show consistently higher amplitudes to the north which is consistent with higher velocity gradients there.

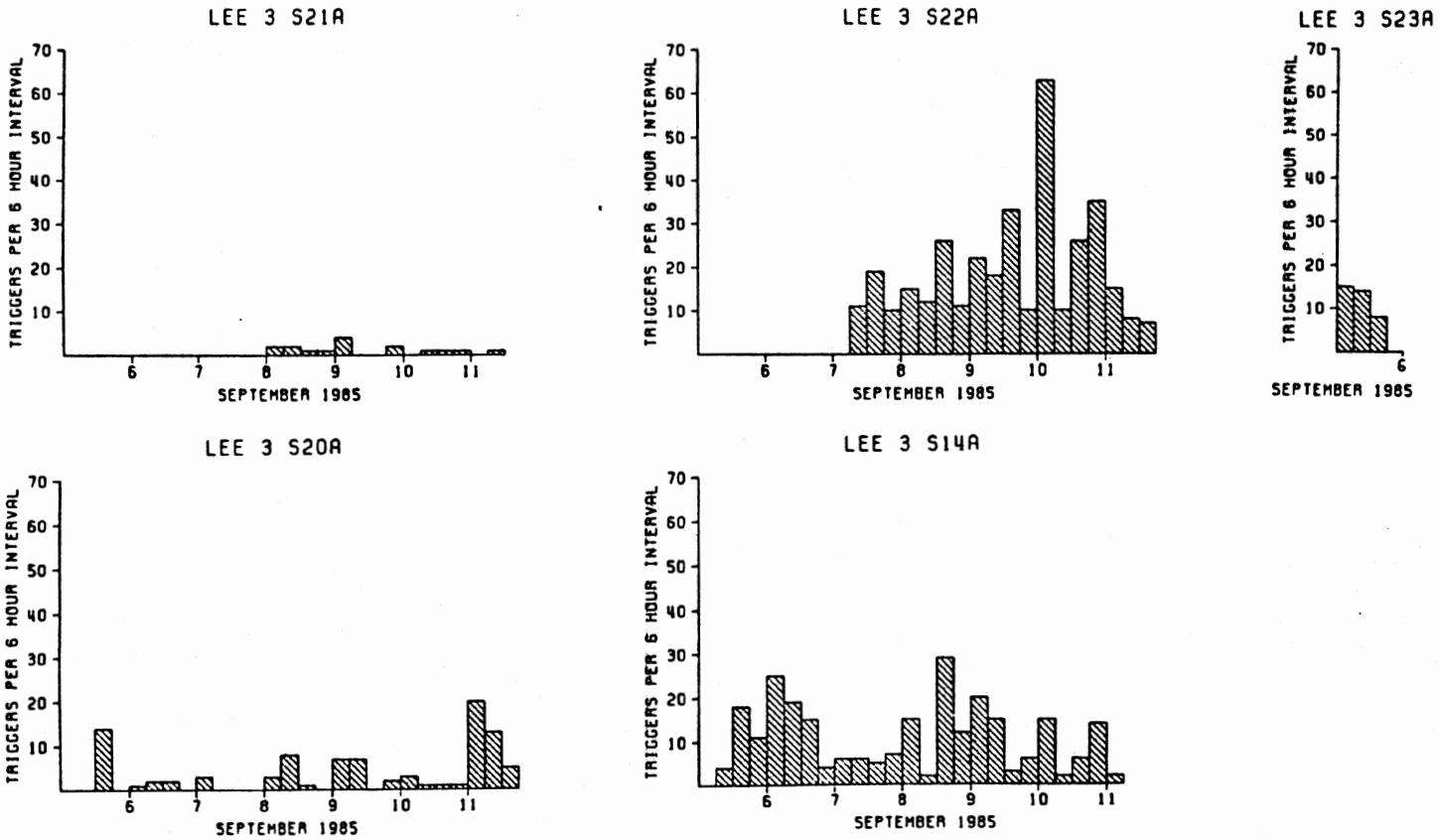

Figure 14. Histograms of activity levels recorded on instruments during the initial deployment on the southern Gorda Ridge.

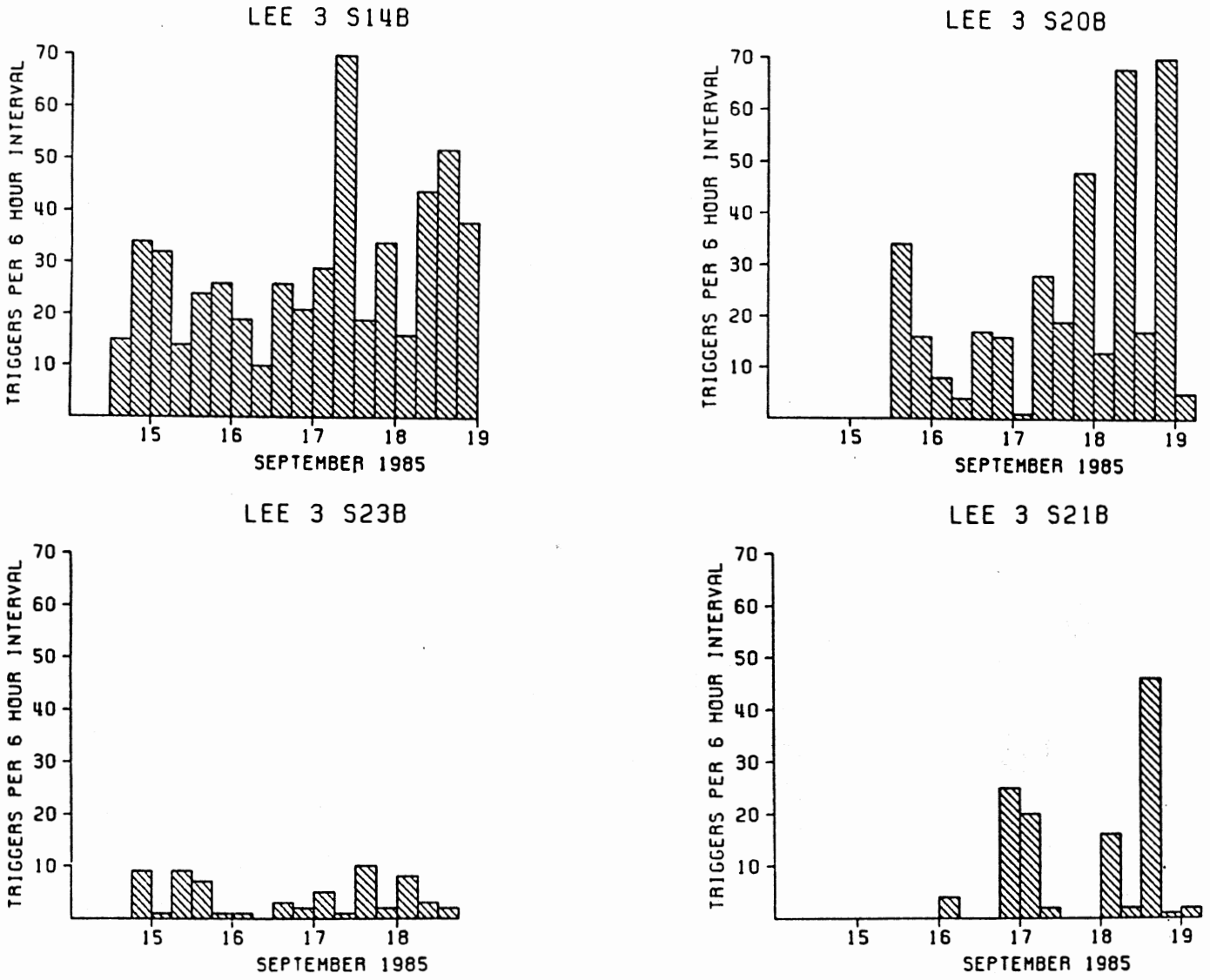

Figure 15. Histograms of activity levels recorded on instruments during the second deployment on the southern Gorda Ridge.

instruments due to tape jams).

On the second deployment (Figure 3), we were able to locate a few more events because more instruments were operating. Two events (the best located of all) were located directly beneath the volcanic center at 40° 53' N. A third was located in the same general area, but slightly to the west where seismic reflection records show a normal fault cutting through to the surface. The only other locatable event was just west of the volcanic center at 41° 06' N. This location is close to the previously deployed station S23A (Figure 2), and may come from the same source as the two events near that station noted above. Figure 16 summarizes the known location of the recorded events.

In general the seismicity levels in the Escanaba trough are low when compared to the northern Gorda Ridge where we could typically locate 1-2 events per hour even with an array having 15 km element spacing. This may be related to the insulating sediment blanket that raises crustal temperatures and results in more ductile than brittle behavior, or it may reflect a different tectonic regime.

Conclusions

1. Results of seismic refraction studies on the Juan de Fuca ridge indicate that porosities are very high in the upper 1.2 km below the seafloor allowing circulation of hydrothermal fluids. Below that depth, porosity is smaller and circulation is probably reduced or confined to fractures. Seismic velocities were slightly lower below the vent field than to the north, suggesting elevated temperatures beneath the vents.

2. Seismic activity in the southern Juan de Fuca vent area was characterized by an intense earthquake swarm that we could not locate. Instruments deployed very near active vents on the ridge axis showed harmonic-tremor-like activity during this event suggesting a magmatic intrusive or eruptive episode was taking place.

3. Seismicity levels in the Escanaba trough are relatively low compared to the northern Gorda Ridge. Many of the recorded events were either from distant earthquakes or the result of biological activity near the instruments. There were indications of seismic activity at 41° 17' N along the axis, but only 6 events could be located with some confidence. Two of these were located on the east valley wall at 40° 45' N. The two most accurately located events were directly beneath the dome at 40° 53' N, and another was located slightly west of there. One event was located slightly to the west of the dome at 41° 06' N. There was no indication of local activity (other than biological) near the volcanic edifice at 41° 00' N, on which our array of instruments was centered.

4. Despite the low levels of seismic activity in the Escanaba trough relative to the northern Gorda Ridge, the recording of a number of locatable events during only two weeks of recording suggests that faults in the area are currently active. Seismic reflection records show a number of faults cutting through the sediments, and some of these correlate with the locations of epicenters that we computed. These active faults are prime targets for future experiments trying to locate active hydrothermal venting sites and massive sulfide deposits.

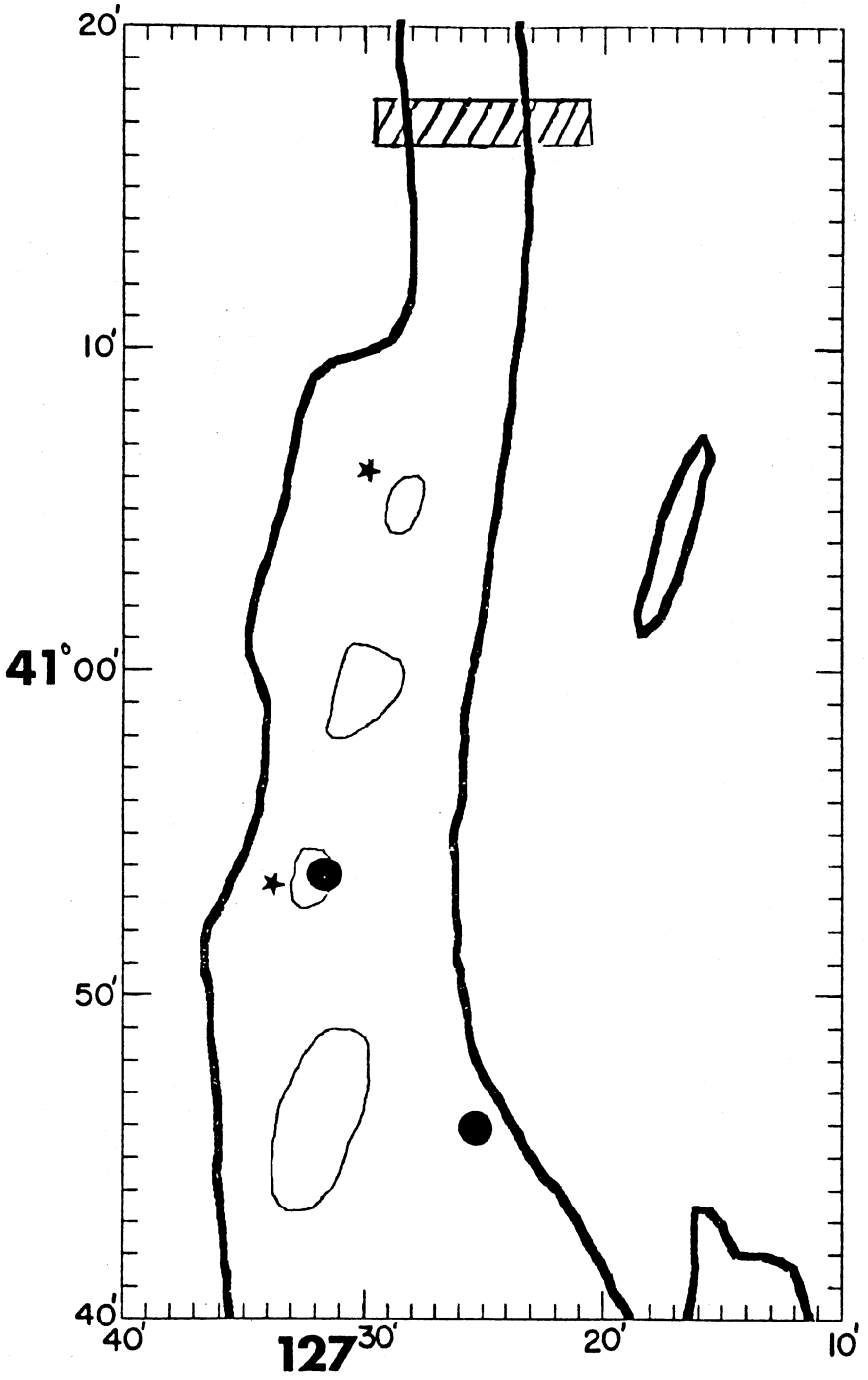

Figure 16. Summary of locations of earthquake epicenters on the southern Gorda Ridge. The heavy lines are the 3000 meter contours defining the axial valley. The light lines are volcanic edifices located from seismic reflection records. The dark circles are places where two events were located at the same place. The stars are single events. The crosshatched box to the north is a region where several events are thought to have originated, but could not be precisely located.

References

Chouet, B.. 1981. Ground motion in the near field of a fluid-driven crack and its interpretation in the study of shallow volcanic tremor. J. Geophys. Res. 86:5985-6016.

Fehler, M., and B. Chouet. 1982. Operation of a digital seismic network on Mt. St. Helens Volcano and observations of long period seismic events that originate under the volcano. Geophysical Research Letters 9:1017-1020.

Morton, Janet L., and Norman H. Sleep. 1985. A mid-ocean ridge thermal model: Constraints on the volume of axial hydrothermal heat flux 90:11345-11354.

Orcutt, J. A., B. L. N. Kennett, and L. M. Dorman. 1976. Structure of the East Pacific Rise from an ocean bottom seismometer survey. Geophys. J. R. Astron. Soc. 45:305-320.

Rona, P. A., G. Klinkhammer, T. A. Nelson, J. H. Trefry, and H. Elderfield. 1986. Black smokers, massive sulphides and vent biota at the Mid-Atlantic Ridge. Nature 321:33-37.